Abdominal Radiology (2019) 44:1395–1406
https://doi.org/10.1007/s00261-018-1847-y

HEPATOBILIARY

Differentiation between inflammatory myofibroblastic tumor and cholangiocarcinoma manifesting as target appearance on gadoxetic acid-enhanced MRI

Amy Inji Chang[1] · Young Kon Kim[1] · Ji Hye Min[2] · Jisun Lee[3] · Honsoul Kim[1] · Soon Jin Lee[1]

Published online: 4 December 2018

Abstract

Purpose To determine the differential features of inflammatory myofibroblastic tumor (IMT) and intrahepatic cholangiocarcinoma (ICC) manifesting as target appearance on gadoxetic acid-enhanced MRI.

Methods Twenty-seven patients with 36 IMTs (1.2–6.0 cm) and 34 patients with 34 ICCs (1.5–6.0 cm) who underwent gadoxetic acid-enhanced MRI were enrolled in this study. Two reviewers evaluated morphology, signal intensity, and enhancement features of tumors on T1-weighted imaging (T1WI), T2-weighted imaging (T2WI), diffusion-weighted imaging (DWI), and gadoxetic acid-enhanced imaging.

Results As for 32 IMTs with target appearance, IMTs most commonly demonstrated early target appearance characterized by a peripheral hypointense rim on unenhanced T1WI (n = 27, 84.4%), central enhanced area with a hypointense rim on arterial phase (AP) and portal venous phase (PVP) (n = 29, 90.6%), and transitional phase (TP) (n = 28, 87.5%). Meanwhile, most of the ICCs showed homogeneous hypointensity on T1WI (100%), a hyperenhancing rim on AP, late target appearance on TP (n = 32, 94.1%) and HBP (n = 32, 94.1%). Target appearance on DWI appearing as hyperintensity with central hypointense area was seen in 2 IMTs and 32 ICCs. On T2WI, 24 IMTs (n = 24, 75.0%) displayed central iso- and peripheral hyperintensity and 27 ICCs (84.4%) showed layered hyperintensity with either brighter or darker area in center. The remaining six IMTs with no target were observed as cystic appearing nodules (n = 3) or ill-defined hypovascular nodules (n = 2) and fibrotic mass (n = 1).

Conclusion IMTs often show early target appearance on unenhanced T1WI, and early dynamic phases of gadoxetic acid-enhanced MRI. Target appearance on later phases, such as TP and HBP, and DWI target appearance were commonly in ICCs, but rare in IMTs.

Keywords Magnetic resonance imaging · Liver tumors · Inflammatory pseudotumor · Cholangiocarcinoma · Target appearance

Introduction

Inflammatory myofibroblastic tumors (IMTs) of the liver are rare benign tumors composed of myofibroblastic mesenchymal spindle cells accompanied by infiltration of plasma cells, lymphocytes, eosinophils, and other inflammatory cells [1]. According to the World Health Organization classification, they are considered as intermediate-grade tumors which have the potential for recurrence after treatment and although rare even distant metastasis can occur. The etiology and pathogenesis of hepatic IMT are poorly documented, but IMT has been reported to be associated with various comorbid

✉ Young Kon Kim
jmyr@dreamwiz.com; youngkon0707.kim@samsung.com

[1] Department of Radiology and Center for Imaging Science, Samsung Medical Center, Sungkyunkwan University School of Medicine, 50, Ilwon-Dong, Kangnam-Ku, Seoul 135-710, Republic of Korea

[2] Department of Radiology, Chungnam National University Hospital, Chungnam National University College of Medicine, Daejeon, Republic of Korea

[3] Department of Radiology, Chungbuk National University Hospital, Cheongju, Republic of Korea

conditions, such as viral or parasitic infections [2], gallstones [3], chronic cholangitis, biliary obstruction, and autoimmune diseases [4].

Several reports have described the imaging findings of IMTs [5–9]. However, these reports seem to be somewhat inconsistent and the characteristic radiological features remain unclear. As a result, on imaging assessment IMTs can be easily mistaken for other benign and malignant lesions, including but not limited to mass-forming intrahepatic cholangiocarcinoma (ICC), hepatocellular carcinoma, or a hepatic abscess [5–8].

Gadoxetic acid (Gd-EOB-DTPA; Primovist ®, Bayer Healthcare) is a widely used magnetic resonance (MR) contrast agent, serving as both an extracellular agent and hepatobiliary agent. In general, ICC is known to appear hypointense on hepatobiliary phase (HBP). But in typical cases the HBP imaging features can be further detailed as an overall hypointense mass demonstrating a relatively hyperintense center (or relatively less hypointense center) surrounded by a truly hypointense rim. This presentation frequently called as the "targetoid appearance" which is considered as an ancillary feature highly specific for ICC [10]. This concept also has been embedded in the Liver Imaging Reporting and Data System (LI-RADS) v2017 which describes about targetoid dynamic enhancement and targetoid appearance on transitional phase (TP) or HBP or diffusion-weighted imaging (DWI) [10].

Meanwhile the concept of targetoid appearance can be quite confusing when it comes to the differentiation between IMT as ICC because both disease entities may present with targetoid appearance on MRI [6, 8, 11–13]. Not surprisingly, IMTs frequently reach the correct diagnosis only after the patient underwent surgical resection [5–7]. Given that IMT can spontaneously regress without treatment, differentiation between IMT and ICC has clinical impact to avoid unnecessary surgery or delayed treatment of ICC with dismal prognosis [14]. Although biopsy could be reliable tool for diagnosis of IMT, it carries sampling error and a risk of complications [15]. To that end, it is worthwhile to elucidate reliable imaging findings that can precisely distinguish between IMT and ICC, and therefore guide to establish optimal strategies for diagnosis and treatment. To the best our knowledge, there has not yet been a study comparing the imaging features between IMT and ICC based on gadoxetic acid-enhanced magnetic resonance imaging (MRI). This study aimed to compare the imaging features of IMT and ICC on gadoxetic acid-enhanced MRI, and therefore elucidate the imaging features that will aid the differential diagnosis.

Materials and methods

Patients

This retrospective study was approved by our institutional review board. Informed consent was waived. We searched our hospital's pathological database between November 2011 and December 2017 using search terms of *"inflammatory myofibroblastic tumor."* A total of 29 patients were identified. Among these patients, we selected 27 IMT patients (16 men and 11 women; age range, 40–71 years; mean, 56.5 years) who had undergone gadoxetic acid MRI. The remaining 2 patients were excluded as they had no MRI examinations. We also searched our hospital's pathological database for patients diagnosed with mass-forming ICC. This query yielded 130 patients. Ninety-six patients were excluded either because (1) the tumor lesions were large (range: 6.2 cm–14.0 cm) and necrotic change seemed to be extensive leading to an overall imaging presentation not typical of targetoid appearance on HBP or DWI (i.e., large central cystic portion) or (2) other ICC features such as peritumoral biliary dilatation, lymph node metastasis, and satellite nodules were obvious. Finally, we included 34 patients (24 men and 10 women; age range, 36–78 years; mean, 61.2 years) with 34 ICCs measuring 6.0 cm or less in diameter. Table 1 shows the size of tumors included in the study. Tumor diameters ranged from 1.2 to 6.0 cm (mean ± SD, 2.83 ± 1.24 cm) in 36 IMTs, and from 1.5 cm to 6.0 cm (mean ± SD, 3.69 ± 1.30 cm)

Table 1 Summary of patient characteristics

	IMT (n = 27)	ICC (n = 34)
Age		
Mean (year)	56.5	61.2
Range (year)	40–71	36–78
Sex		
Male	16	24
Female	11	10
Size		
Range (cm)	1.2–6.0	1.5–6.0
Mean ± SD (cm)	2.83 ± 1.24	3.69 ± 1.30
Number		
Single	20	34
Multiple	7	0
CA 19-9 (U/ml)[a]	4.0 (1.2–65.0)	17.0 (1.2–177.0)
Symptom	Fever (n = 2)	Fever (n = 1)
	Weight loss (n = 2)	

IMT inflammatory myofibroblastic tumor, *ICC* intrahepatic cholangiocarcinoma

[a]Data are medians, with the range in parentheses

in 34 ICCs. To be more specific, 26 IMTs and 20 ICCs were smaller than 3 cm in diameter.

Reference standard

The histopathologic diagnosis of IMT was confirmed with surgical specimens in 4 lesions of 3 patients, and by percutaneous biopsy in the remaining 24 patients. All 34 ICCs were confirmed on surgical specimens. The average time interval between MR examination and surgery was 15 days (range, 7–25 days). The patients who received surgery underwent segmentectomy (n = 7), bisegmentectomy (n = 10) or lobectomy (n = 20).

MR examination

All MRI scans were acquired using an Intera Achieva 3.0-T whole-body MR system (Philips Healthcare, Best, The Netherlands) equipped with a dual-source parallel radiofrequency transmission system and a 16-channel phased-array coil used as the receiver coil. Baseline MRI included T1-weighted turbo field-echo in-phase and opposed sequence (TR/first echo TE, second echo TE, 10/2.3 [in-phase], 3.45 [opposed-phase]; flip angle, 15°; matrix size, 256 × 194; bandwidth, 434.3 Hz/pixel), breath-hold multishot T2-weighted sequence with an acceleration factor of 2 (1796/70; flip angle, 90°; matrix size, 324 × 235; bandwidth, 258.4 Hz/pixel), and respiratory-triggered single-shot heavily T2-weighted sequence with an acceleration factor of 2 (1802/160; flip angle, 90°; matrix size, 252 × 254; bandwidth, 420.9 Hz/pixel) with 5 mm section thickness and 32–38-cm field of view.

For gadoxetic acid-enhanced imaging, unenhanced, arterial phase (AP, 20–35 s), portal venous phase (PVP, 60 s), 3-min transitional phase (TP), and 20-min HBP were obtained using T1-weighted 3D turbo field-echo sequence (enhanced T1 high-resolution isotropic volume examination; eTHRIVE, Philips Healthcare) (3.1/1.5; flip angle, 10°; matrix size, 256 × 256; bandwidth, 724.1 Hz/pixel) with a 2 mm section thickness and 32–38 cm field of view. Measured voxel size was 1.5 × 1.5 × 4.0 mm and reconstructed voxel size was 1.17 × 1.17 × 2.0 mm. Contrast agent was automatically administered intravenously at a rate of 1 mL/s for a dose of 0.025 mmol/kg body weight using a power injector, followed by a 20-mL saline flush.

Diffusion-weighted single-shot echo planar imaging with simultaneous respiratory triggering was performed using TR/TE of 1600/70 ms. Scanning parameters were as follows: b value 0, 100, and 800 s/mm^2; spectral presaturation with inversion recovery for fat suppression; matrix size, 100 × 100; acceleration factor of SENSE, 2.0; field of view, 35 × 35 cm; number of excitations, 4; slice thickness, 5 mm; slice gap, 1 mm; and axial slices, 33. The apparent diffusion coefficient was calculated by a mono-exponential function using b values of 100 and 800 s/mm^2.

Image analysis

Two gastrointestinal radiologists (@ and @, with 11 and 18 years of experience in liver MRI, respectively) reviewed MRIs on a picture archiving and communication system (Pathspeed, GE Medical Systems Integrated Imaging Solutions, Mt. Prospect, IL, USA). The two observers independently evaluated (1) the shape of tumors, (2) signal intensity of tumors relative to liver parenchyma on precontrast T1-weighted imaging (T1WI), T2-weighted imaging (T2WI), (3) enhancement pattern or signal intensity focusing on targetoid appearance on gadoxetic acid-enhanced imaging including AP, PVP, TP, and HBP, and b-800 diffusion-weighted imaging (DWI) [11]. After independently evaluating the images, the two observers then jointly evaluated the results with discrepancy until a consensus was reached.

Results

Baseline clinical characteristics

Table 1 shows the clinical features of study populations and tumors included in the study. Four patients had chronic hepatitis associated with viral hepatitis B. In case of the 27 IMT patients, two patients had four lesions, five patients had two lesions, and the remaining 20 patients each had one lesion. All patients with ICCs had a single tumor. Twenty-four ICCs (70.6%) were considered to be moderately differentiated, while 10 (29.4%) were poorly differentiated. Thirty ICC (88.2%) lesions presented with more or less necrosis (range 5–55%), with a median value of 20% necrosis.

MRI features

MRI features of IMTs and ICCs manifesting as target appearance are summarized in Table 2. In addition, the representative signal intensity patterns of tumors at each MR sequence are also shown in Fig. 1. Of the tumors, 33 IMTs (86.8%) and 33 ICCs (97.1%) showed lobulated or wavy contours, while the contours of the other tumors were smooth.

MRI features of IMTs with target appearance

IMTs most commonly had an early target appearance characterized by central isointensity and a peripheral hypointense rim on unenhanced T1WI (n = 27, 84.4%),

Table 2 Summary of imaging characteristics of IMT and ICC showing targetoid appearance

	IMT (n = 32)	ICC (n = 34)
T1WI		
Hypointensity	5[a]	34
Target	27	0
T2WI		
Moderate hyperintensity (central brightness)	8	7
Layered	24	Central brightness (7), darkness (12), both (8)
AP		
Hyperintense rim	3	34
Target	29 (5, 24)	0
TP		
Hypointensity	4	2
Target	28	32
HBP		
Hypointensity	30	2
Target	2	32
DWI		
Hyperintensity	30	2
Target	2	32
Central dot	18	0

IMT inflammatory myofibroblastic tumor, *ICC* intrahepatic cholangiocarcinoma, *AP* arterial phase, *TP* transitional phase, *HBP* hepatobiliary phase

Target appearance on pre-and postcontrast T1WI (AP, TP, and HBP) consisted of central enhancement and peripheral hypointense rim. Target appearance on DWI consisted of central hypointense area within hyperintensity. Data in parentheses represent number of lesion with central hyperintensity and lesion with central isointensity, respectively

[a]Hypointensity in IMTs is not clear as in ICCs

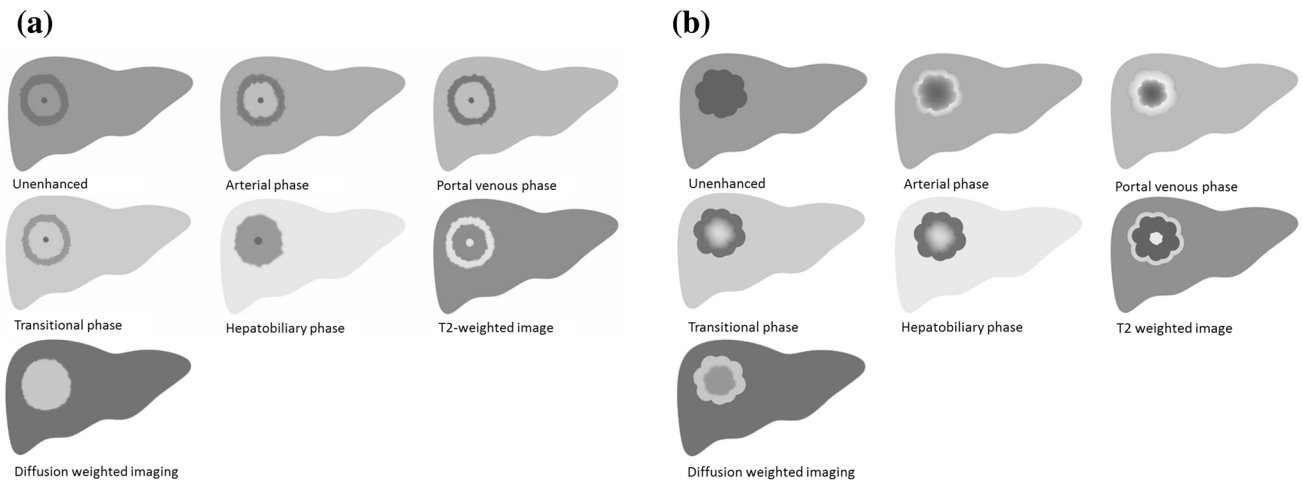

Fig. 1 Schematic picture explaining the image patterns of inflammatory myofibroblastic tumor (**a**) and intrahepatic cholangiocarcinoma (**b**) on gadoxetic acid-enhanced MRI

central enhancement and a peripheral hypointense rim on AP, PVP (n = 29, 90.6%), and TP (n = 28, 87.5%) (Fig. 2), respectively. Consequently, the thin hypointense rim responsible for the target appearance was persistently seen in 27 IMTs (84.4%) from unenhanced T1WI to TP. On AP imaging, the degree of enhancement of the central portion was comparable to that of the background liver in 24 IMTs (Fig. 2), while five IMTs showed relatively

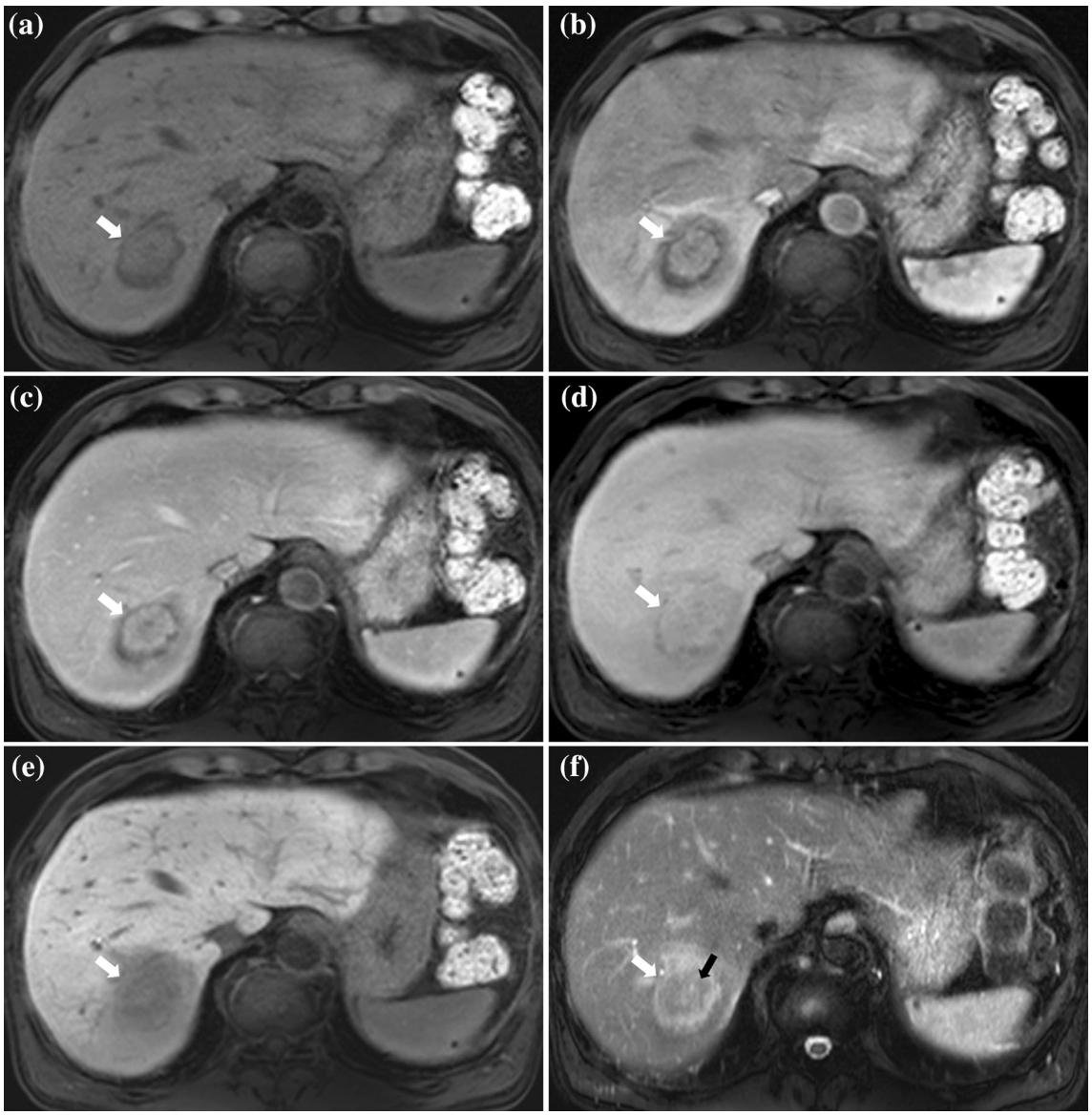

Fig. 2 A 3.5-cm inflammatory myofibroblastic tumor in a 63-year-old man. On axial fat-suppressed T1-weighted 3D gradient echo images obtained during **a** unenhanced phase, **b** arterial phase, **c** portal venous phase, and **d** 3-min transitional phase (**d**), a tumor with a mildly lobulated contour (arrows) shows an early target appearance (a central isointense area with a peripheral hypointense rim relative to the liver parenchyma). **e** On 20-min HBP, the tumor (arrow) appears as a hypointense mass. **f** On T2-weighted imaging, the tumor (arrow) also shows a layered appearance consisting of an inner isointense area (black arrow) and a hyperintense outer rim relative to the liver parenchyma. Note the tiny dot in the center of the tumor

stronger enhancement than that of the liver (Fig. 3). On TP imaging, rim-like enhancement was seen in the remaining four IMTs including three lesions with rim enhancement that was identifiable from AP to TP (Fig. 4). On HBP imaging, most IMTs ($n = 30$, 93.8%) presented as hypointense but still two lesions showed a target appearance consisting of central enhancement with a peripheral hypointense rim. On T2WI, 24 IMTs ($n = 24$, 75.0%) showed central isointensity similar to that of the background liver parenchyma and peripheral hyperintensity (Figs. 2, 3). A tiny central dot was frequently observed which appeared hypointense on T1WI in 18 IMTs and on T2WI hyperintense in 15 IMTs (Figs. 2, 3).

MRI features of IMTs without target appearance

Out of six IMTs that showed no targetoid appearance, three had wide area of central brightness on T2WI mimicking cavity or cystic component that showed no enhancement. They had peripheral rind that was nearly isointense on unenhanced T1WI, AP, and PVP and hypointense on TP and HBP compared to signal intensity of background liver.

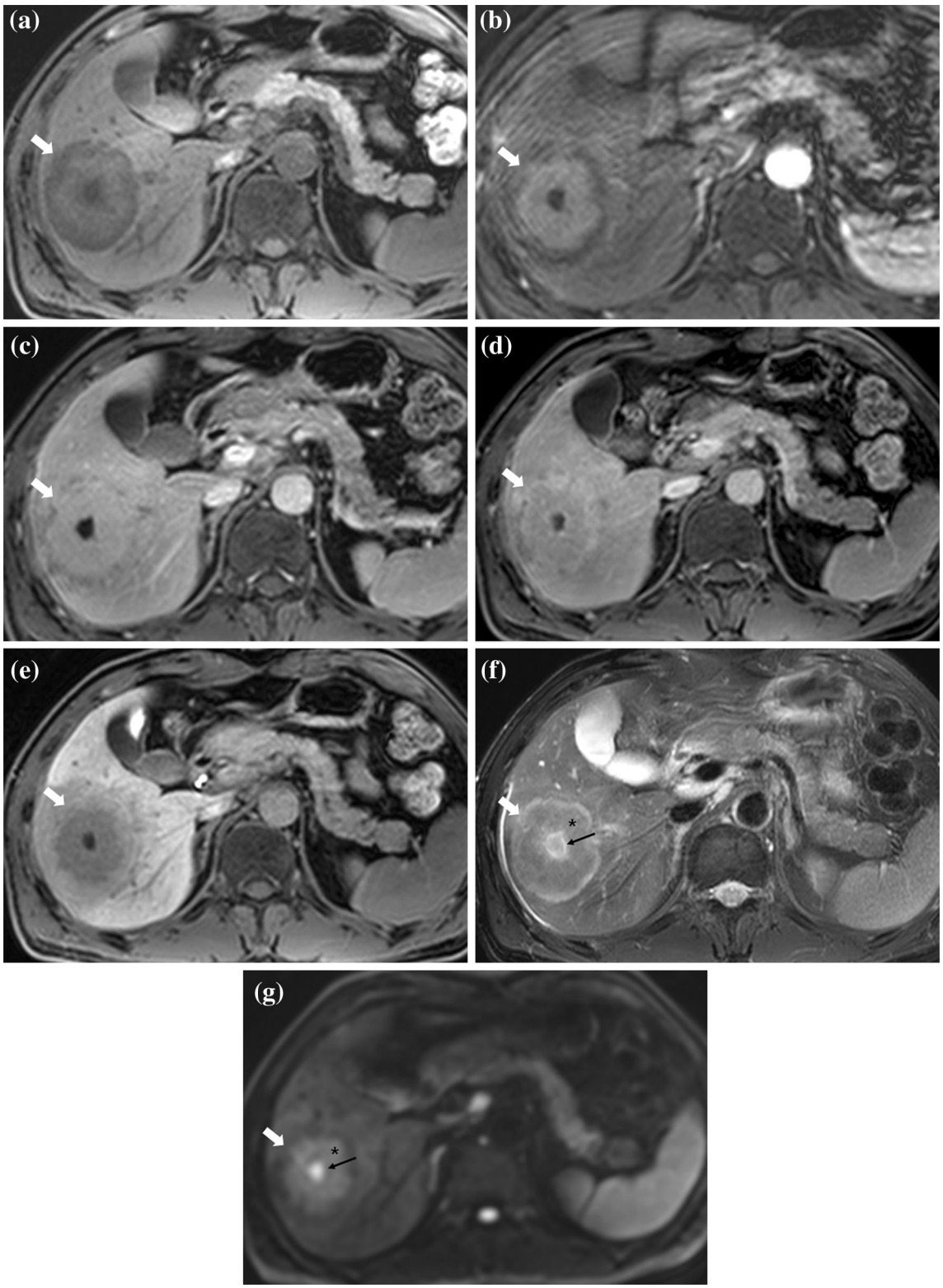
(a)
(b)
(c)
(d)
(e)
(f)
(g)

◀**Fig. 3** A 6.0-cm inflammatory myofibroblastic tumor in a 57-year-old man. On axial fat-suppressed T1-weighted 3D gradient echo images obtained during **a** unenhanced phase, **b** arterial phase, and **c** portal venous phase after gadoxetic acid administration, a tumor with mildly lobulated contour (arrows) shows an early target appearance of (a central iso- or hyperintense area with a peripheral hypointense rim relative to the liver parenchyma). **d** On transitional phase imaging, the tumor (arrow) is seen as an iso- or hypointense inner zone with a hyperintense outer rim. **e** On 20-min HBP, the tumor (arrow) is seen as a hypointense mass. **f** On T2-weighted and **g** diffusion-weighted imaging at $b = 800$ s/mm^2, the tumor (arrow) shows inner isointense area (asterisk) and a hyperintense outer rim relative to the liver parenchyma. Note the tiny dot (black arrow) in the center of the tumor

Two IMTs were seen as ill-defined irregular shaped nodular lesion that showed subtle hypointensity on unenhanced and enhanced T1WIs and subtle hyperintensity on T2WI and DWI with no obvious enhancement. The remaining one was observed as round fibrotic mass that showed dark signal intensity on T2WI and hypointensity on unenhanced and enhanced T1WIs.

MRI features of ICCs

All ICCs showed homogeneous hypointensity on precontrast T1WI and a hyperenhancing peripheral rim with various thicknesses on AP imaging (Fig. 5). Late target appearance was observed in 32 ICCs (94.1%) on TP and HBP imaging (Fig. 6) In addition, a non-enhancing defect was present in the center of tumors which seemed to correspond to a region of extensive tumor necrosis in 25 ICCs (73.5%) (Fig. 4). On T2WI, 27 ICCs (84.4%) showed layered hyperintensity accompanying a central brighter or darker area that seemed to reflect the presence of fibrous stroma accompanying varying degrees of necrosis.

On DWI, 32 ICCs (94.1%) showed target appearance presenting with a relatively darker area in the central portion of an overall hyperintense tumor (Fig. 5). Meanwhile, only two IMTs had a target appearance on DWI.

Interobserver agreement for MRI findings

The κ values between the two observers in assigning target appearance were 0.938 for T1WI, 0.908 for AP, 0.626 for TP, 0.817 for HBP, and 0.770 for DWI, indicating substantial to excellent degree of agreement.

Discussion

The reported imaging findings of IMTs in the literature appears to be inconsistent and non-specific, and considerable overlap exists with those of ICCs, HCCs, or even abscesses [16]. In this study, we focused on IMTs which demonstrate targetoid appearance on gadoxetic acid-enhanced MRI, for such feature can closely mimic the imaging presentation of ICC. The most prominent finding in our study was that IMTs had a tendency to demonstrate target appearance at the early part of dynamic study (unenhanced T1WI and dynamic phases from AP to TP, but not the HBP). Meanwhile, target appearance of ICCs usually appeared only on TP and HBP.

The etiology and pathogenesis of hepatic IMT are not fully understood. A fundamental question in the pathogenesis of IMT is whether this disease entity is inflammatory or neoplastic in nature. Matsubara et al. [17] proposed to categorize pulmonary inflammatory pseudotumors into 3 major histologic subtypes: (1) organizing pneumonia type, (2) fibrohistiocytoma type, and (3) lymphoplasmacytic type. Such concept is similar in line with the view point that hepatic IMTs are associated with different underlying comorbidities, such as viral or parasitic infections [2], gallstones [3], chronic cholangitis, biliary obstruction, and autoimmune diseases [4]. We have speculated that the IMT cases in our study are more likely inflammatory lesions and not neoplasms for a few reasons. First, with the exception of three patients who underwent surgical resection, spontaneous regression of the mass occurred within 2 months even without any treatment. This implies that the lesions were inflammatory lesions. Second, even with the use of gadoxetic acid-enhanced MRI, the image findings of our cases overlap with those of solid organizing abscesses which also demonstrate early target appearance: central enhancement and a peripheral hypoattenuated or hypointense rim on AP of computed tomography (CT) or MRI, followed by central low attenuation or a hypointense area with an enhancing peripheral rim on 3-min delayed-phase imaging [8, 18, 19]. However, the TP partly possess features of HBP and therefore is distinct from the equilibrium phase of CT or MRI which uses extracellular contrast agent. The wider inner portion of solid organizing abscess could be interpreted as a granulation tissue with hypervascularity that is seen as enhancing area which is hyperintense or isointense relative to liver parenchyma [18]. In addition, given that granulation tissue approximates normal liver tissue during the healing process, the signal intensity on unenhanced T1- and T2WI are similar to that of normal liver parenchyma as shown in most of our cases [18]. In addition, a central tiny cystic space was noted in some cases of IMT as well as solid organizing abscess, which probably represents remnant necrotic space [18].

Three IMTs in our study were observed as wavy-contoured masses that showed early rim-like enhancement followed by progressive gradual enhancement that retained the rim-like enhancement pattern on PVP and TP. Interestingly, on unenhanced T1WI, these cases were almost

isointense without hypointense rim and not clearly delineated, which are features that are not frequently observed in typical ICC. Meanwhile, it has been reported that inflammatory conditions more often appear as isointense on unenhanced T1WI [20]. Such features along with the fact that IMT lacks late target appearance and DWI target appearance may be exploited to differentiate IMT from ICC. The target appearance on DWI is now considered to be an ancillary feature for ICC. In our study, only two IMTs had a target appearance on DWI. Due to the inherent T2 characteristics in DWI (T2 shine-through or T2 black

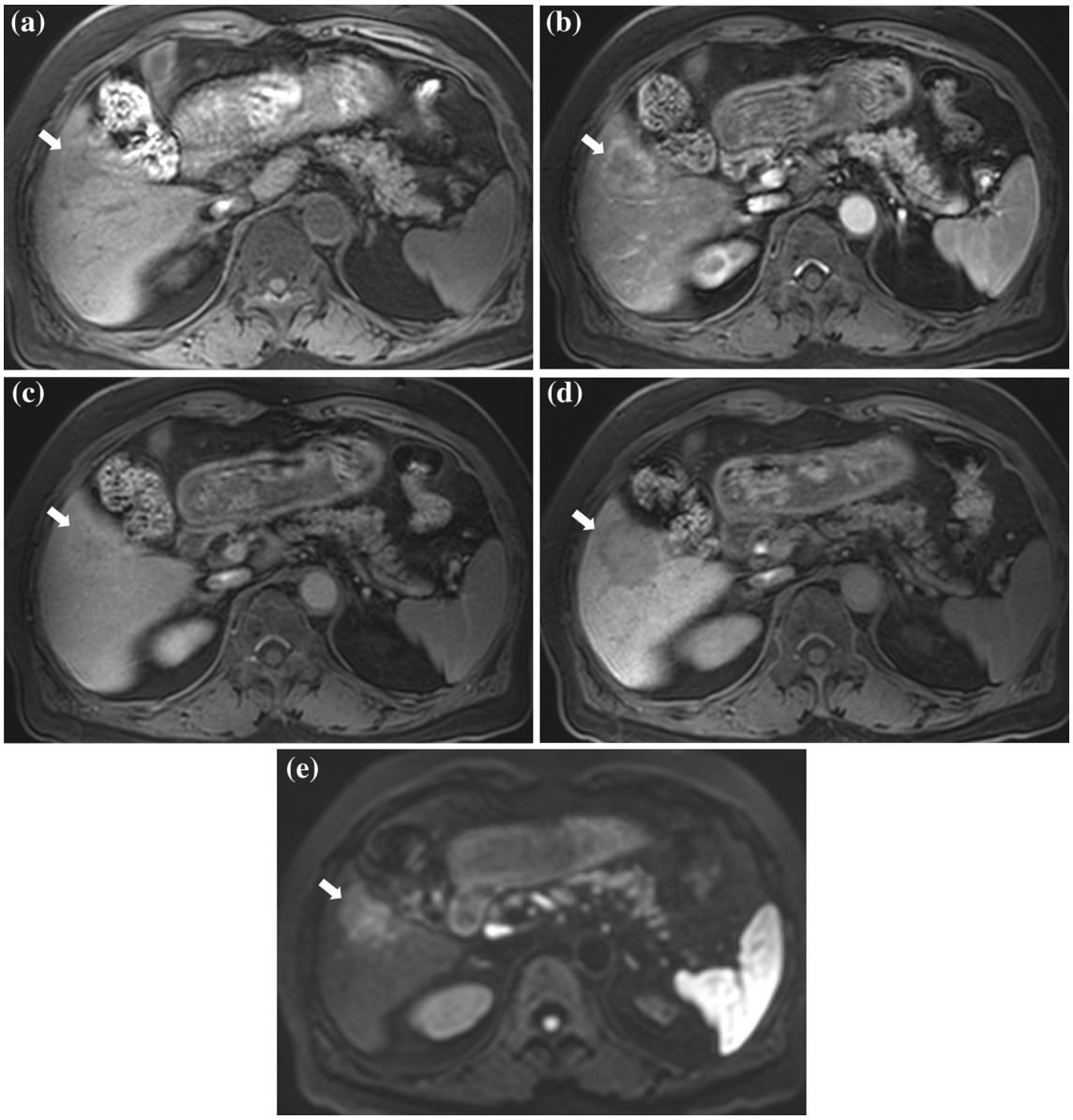

Fig. 4 A 3.5-cm inflammatory myofibroblastic tumor in a 75-year-old woman. On axial fat-suppressed T1-weighted 3D gradient echo images obtained during **a** unenhanced phase, **b** arterial phase, **c** transitional phase, and **d** hepatobiliary phase after gadoxetic acid administration, a tumor with a wavy contour (arrows) shows early peripheral hyperenhancement followed by a late target appearance on HBP. Note that the lesion is not clearly seen on unenhanced T1-weighted imaging. **e** On diffusion-weighted imaging at $b = 800$ s/mm^2, the tumor (arrow) does not show a target appearance

Fig. 5 A 4.0-cm intrahepatic cholangiocarcinoma in a 62-year-old man. On axial fat-suppressed T1-weighted 3D gradient echo images obtained during **a** unenhanced phase, **b** arterial phase, **c** portal venous phase, **d** transitional phase, and **e** hepatobiliary phase after gadoxetic acid administration, a tumor with a wavy contour (arrows) shows early peripheral hyperenhancement followed by a late target appearance (central enhancement and a hypointense rim on transitional phase and hepatobiliary phase). Note the central hypointense area representing necrosis. **f** On T2-weighted imaging, a central darker area indicating fibrosis is observed. **g** On diffusion-weighted imaging at $b = 800$ s/mm^2, the tumor (arrow) also shows a target appearance consisting of a central darker area and a hyperintense periphery ▶

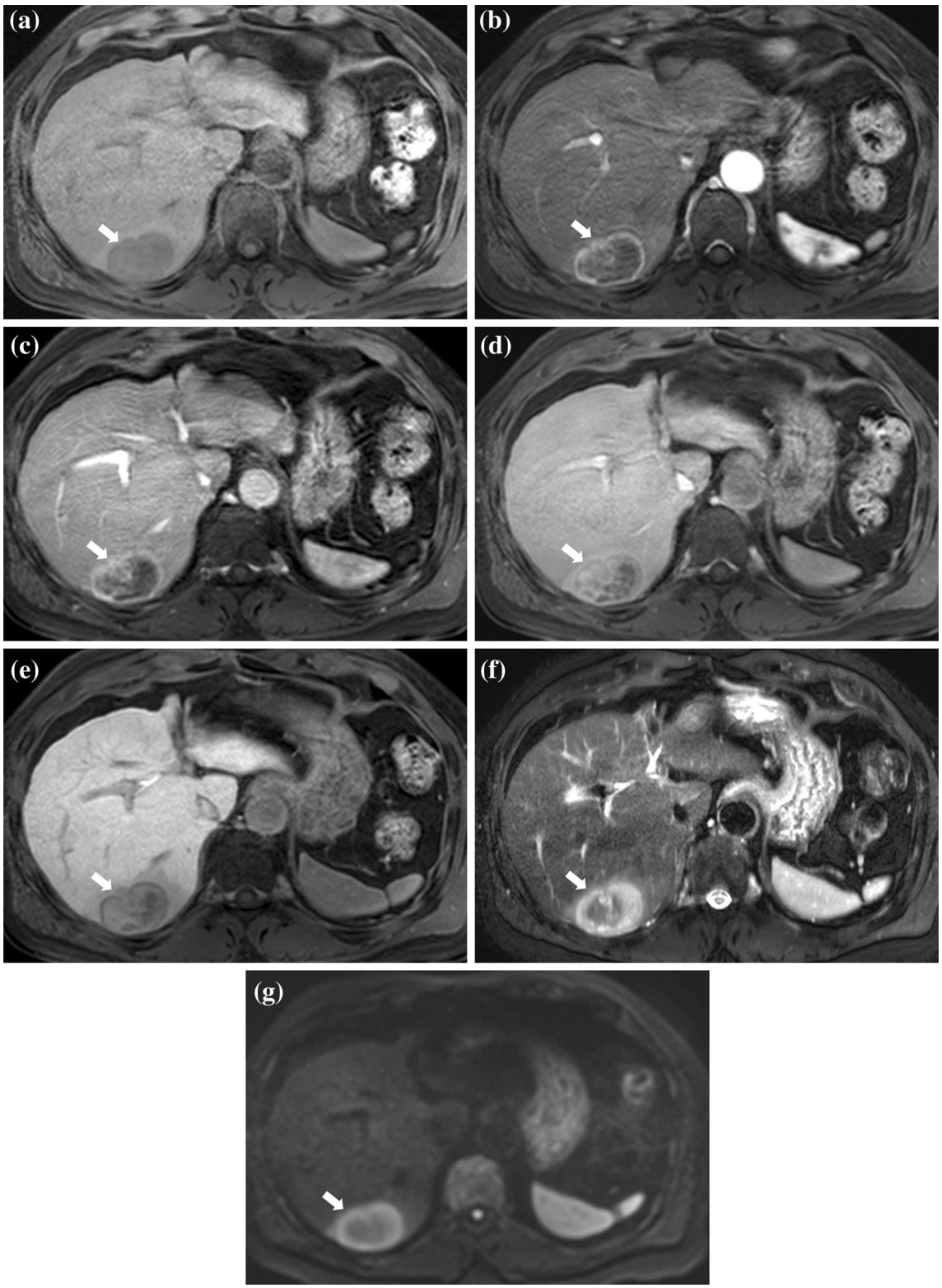
(a)
(b)
(c)
(d)
(e)
(f)
(g)

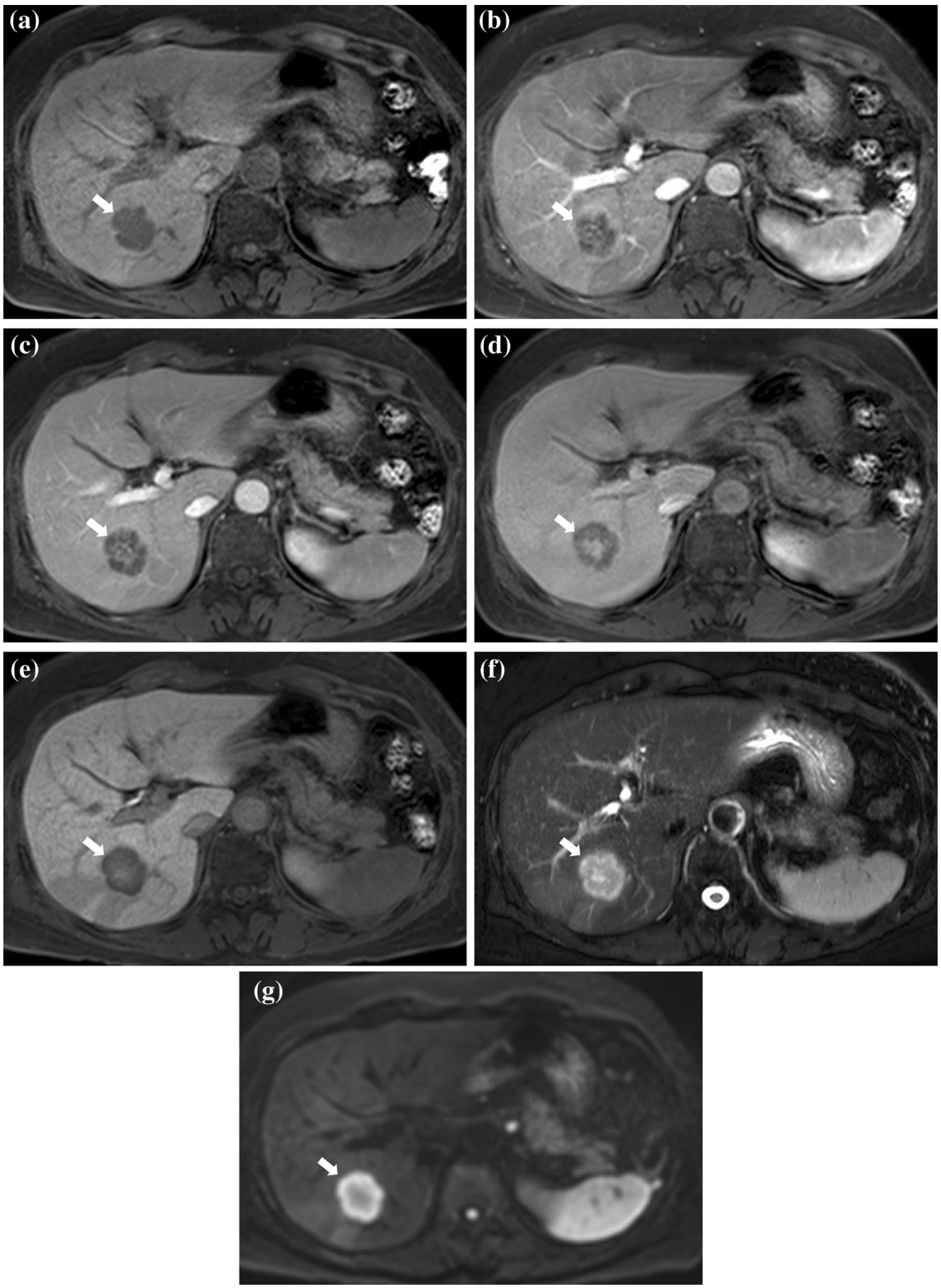

Fig. 6 A 2.0-cm intrahepatic cholangiocarcinoma in a 68-year-old woman. On axial fat-suppressed T1-weighted 3D gradient echo images obtained during **a** unenhanced phase, **b** arterial phase, **c** portal venous phase, **d** transitional phase, and **e** hepatobiliary phase after gadoxetic acid administration, a tumor with a wavy contour (arrows) shows early peripheral hyperenhancement followed by a late target appearance (central enhancement and a hypointense rim on transitional phase and hepatobiliary phase). **f** On T2-weighted imaging, a central darker and bright area indicating fibrosis are observed. **g** On diffusion-weighted imaging at $b = 800$ s/mm^2, the tumor (arrow) also shows a target appearance consisting of a central darker area and a hyperintense periphery

out), two IMTs exhibit a target appearance on DWI due to the inherent layered appearance on T2WI [21].

The central fibrotic component of ICC can exhibit variable signal intensity on T2WI according to the maturation and amount of collagen, of which component is responsible for the central enhancement within the mass contributing to the late target appearance on HBP and TP [22, 23]. Meanwhile, the peripheral cellular area of ICC exhibits rim enhancement on AP due to rich tumor vascularity which later converts to become a hypointense rim which consequently produces the late target appearance on HBP. Smaller ICCs tend to have less fibrotic components and higher cellular areas which in turn appear as hypervascular tumors on AP mimicking HCC [23] or IMTs. This is the main reason why we have chosen relatively smaller ICCs for comparison. When using extracellular contrast agent, central enhancement within ICC is usually seen at the ultradelayed phase acquired at 5 min or later [24]. However, in our study most ICCs (n = 32) demonstrated a late target appearance on 3-min TP as well as HBP. We believe that this phenomenon reflects the short blood half-life of gadoxetic acid.

This study is descriptive in nature and did not examine the diagnostic performance on differentiation between IMT and ICC. However, the results of our study present a clear contrast between the two disease entities that both present with target appearance at slightly different phases on gadoxetic acid-enhanced MRI. For differentiating between IMTs and ICCs with target appearance, when we apply early target appearance, we can achieve 90.6% (n = 29/32) of sensitivity and 100% specificity for identifying IMTs. As for three lesions showing early rim-enhancing pattern, application of nearly isointensity on unenhanced T1WI and lack of DWI target and late target appearance can lead to correct diagnosis of IMTs.

Several limitations of this study should be noted. First, because this was a retrospective study, it may have some inherent selection bias. As previously described since we focused on tumors with targetoid appearance while focusing on the possible effects of tumor size, we included relatively smaller ICCs. Second, our study is descriptive for a selected case series and thereby compared the imaging features of two disease entities. Thus, we provided no statistical data regarding the diagnostic performance of the differential features. Third, we did not include other types of hepatic tumors. The binary distinction between IMT and ICC might oversimplify the clinical scenario. Nevertheless, in clinical practice, accurate differentiation between IMT and ICC is a concern. Fourth, we did not address the question of whether IMT is an inflammatory lesion or a true neoplasm. The pathological comparison between IMT and solid organizing abscesses should be studied in the future. Fifth, this study shares the intrinsic limitations of any consensus review.

In conclusion, IMTs often show early target appearance on unenhanced T1WI and early dynamic phases of gadoxetic acid-enhanced MRI. Meanwhile, ICCs tended to demonstrate late target appearance on TP and HBP, and target appearance on DWI.

Compliance with ethical standards

Conflict of interest The authors declared that they have no conflict of interest.

Ethical approval All procedures performed in studies involving human participants were in accordance with the ethical standards of the institutional and/or national research committee and with the 1964 Helsinki declaration and its later amendments or comparable ethical standards.

Informed consent Informed consent was waived by IRB.

References

1. Yamamoto H, Yamaguchi H, Aishima S, Oda Y, Kohashi K, Oshiro Y, Tsuneyoshi M (2009) Inflammatory myofibroblastic tumor versus IgG4-related sclerosing disease and inflammatory pseudotumor: a comparative clinicopathologic study. Am J Surg Pathol 33:1330–1340. https://doi.org/10.1097/PAS.0b013e3181a5a207
2. Pannain VL, Passos JV, Rocha Filho A, Villela-Nogueira C, Caroli-Bottino A (2010) Agressive inflammatory myofibroblastic tumor of the liver with underlying schistosomiasis: a case report. World J Gastroenterol 16:4233–4236. https://doi.org/10.3748/wjg.v16.i33.4233
3. Al-Jabri T, Sanjay P, Shaikh I, Woodward A (2010) Inflammatory myofibroblastic pseudotumour of the liver in association with gall stones - a rare case report and brief review. Diagn Pathol 5:53. https://doi.org/10.1186/1746-1596-5-53
4. Papachristou GI, Wu T, Marsh W, Plevy SE (2004) Inflammatory pseudotumor of the liver associated with Crohn's disease. J Clin Gastroenterol 38:818–822. https://doi.org/10.1016/j.crohns.2009.06.005
5. Iguchi H, Yamazaki H, Tsunoda H, Takahashi Y, Yokomori H (2013) A Case of Inflammatory Pseudotumor of the Liver Mimicking Hepatocellular Carcinoma on EOB-MRI and PET. Case Rep Med 2013:594254. https://doi.org/10.1155/2013/594254
6. Bae SK, Abiru S, Kamohara Y, Hashimoto S, Otani M, Saeki A, Nagaoka S, Yamasaki K, Komori A, Ito M, Fujioka H, Yatsuhashi H (2015) Hepatic inflammatory pseudotumor associated with xanthogranulomatous cholangitis mimicking cholangiocarcinoma. Inter Med 54:771–775. https://doi.org/10.2169/internalmedicine.54.2623
7. Deng FT, Li YX, Ye L, Tong L, Yang XP, Chai XQ (2010) Hilar inflammatory pseudotumor mimicking hilar cholangiocarcinoma. Hepatobiliary Pancreat Dis Int 9:219–221
8. Xiao Y, Zhou S, Ma C, Luo J, Zhu H, Tang F (2013) Radiological and histopathological features of hepatic inflammatory myofibroblastic tumour: analysis of 10 cases. Clin Radiol 68:1114–1120. https://doi.org/10.1016/j.crad.2013.05.097

9. Park HJ, Kim YK, Park MJ, Lee WJ (2013) Small intrahepatic mass-forming cholangiocarcinoma: target sign on diffusion-weighted imaging for differentiation from hepatocellular carcinoma. Abdom Imaging 38:793–801. https://doi.org/10.1007/s00261-012-9943-x
10. Elsayes KM, Hooker JC, Agrons MM, Kielar AZ, Tang A, Fowler KJ, Chernyak V, Bashir MR, Kono Y, Do RK, Mitchell DG, Kamaya A, Hecht EM, Sirlin CB (2017) 2017 Version of LI-RADS for CT and MR Imaging: An Update. Radiographics 37:1994–2017. https://doi.org/10.1148/rg.2017170098
11. Karahan OI, Isin S, Baykara M, Coskun A (2003) Case report: Inflammatory pseudotumor of the liver with target-like appearance. Tani Girisim Radyol 9:75–77
12. Min JH, Kim YK, Choi SY, Jeong WK, Lee WJ, Ha SY, Ahn S, Ahn HS (2017) Differentiation between cholangiocarcinoma and hepatocellular carcinoma with target sign on diffusion-weighted imaging and hepatobiliary phase gadoxetic acid-enhanced MR imaging: Classification tree analysis applying capsule and septum. Eur J Radiol 92:1–10. https://doi.org/10.1016/j.ejrad.2017.04.008
13. Yu JS, Park C, Kim JH, Chung JJ, Kim KW (2007) Inflammatory myofibrobalstic tumors in the liver: MRI of two immunohistochemically-verified cases. J Mag Reson Imaging 26:418–421
14. Zhao JJ, Ling JQ, Fang Y, Gao XD, Shu P, Shen KT, Qin J, Sun YH, Qin XY (2014) Intra-abdominal inflammatory myofibroblastic tumor: spontaneous regression. World J Gastroenterol 20:13625–13631. https://doi.org/10.3748/wjg.v20.i37.13625
15. Eun HW, Kim JH, Hong SS, Kim YJ (2012) Malignant versus benign hepatic masses in patients with recurrent pyogenic cholangitis: MR differential diagnosis. Abdom Imaging 37:767–774. https://doi.org/10.1007/s00261-011-9833-7
16. Matsubara O, Tan-Liu NS, Kenney RM, Mark EJ (1988) Inflammatory pseudotumors of the lung: progression from organizing pneumonia to fibrous histiocytoma or to plasma cell granuloma in 32 cases. Hum Pathol 19:807–814. https://doi.org/10.1016/S0046-8177(88)80264-8
17. Kim YK, Kim CS, Lee JM, Ko SW, Moon WS, Yu HC (2006) Solid organizing hepatic abscesses mimic hepatic tumor: Multiphasic computed tomography and magnetic resonance imaging findings with histopathologic correlation. J Comput Assist Tomogr 30:189–196
18. Kang TW, Kim SH, Jang KM, Choi D, Choi JY, Park CK (2014) Inflammatory myofibroblastic tumours of the liver: gadoxetic acid-enhanced and diffusion-weighted MRI findings with 18F-FDG PET/CT and clinical significance of regression on follow-up. Clin Radiol 69:509–518. https://doi.org/10.1016/j.crad.2013.12.018
19. Kim YK, Lee YH, Kim CS, Lee MW (2011) Differentiating focal eosinophilic liver disease from hepatic metastases using unenhanced and gadoxetic acid-enhanced MRI. Abdom Imaging 36:425–432. https://doi.org/10.1007/s00261-011-9752-7
20. Hiwatashi A, Kinoshita T, Moritani T, Wang HZ, Shrier DA, Numaguchi Y, Ekholm SE, Westesson PL (2003) Hypointensity on diffusion-weighted MRI of the brain related to T2 shortening and susceptibility effects. AJR Am J Roentgenol 181:1705–1709. https://doi.org/10.2214/ajr.181.6.1811705
21. Maetani Y, Itoh K, Watanabe C, Shibata T, Ametani F, Yamabe H, Konishi J (2001) MR imaging of intrahepatic cholangiocarcinoma with pathologic correlation. AJR Am J Roentgenol 176:1499–1507. https://doi.org/10.2214/ajr.176.6.1761499
22. Chong YS, Kim YK, Lee MW, Kim SH, Lee WJ, Rhim HC, Lee SJ (2012) Differentiating mass-forming intrahepatic cholangiocarcinoma from atypical hepatocellular carcinoma using gadoxetic acid-enhanced MRI. Clin Radiol 67:766–773. https://doi.org/10.1016/j.crad.2012.01.004
23. Kim SH, Lee CH, Kim BH, Kim WB, Yeom SK, Kim KA, Park CM (2012) Typical and atypical imaging findings of intrahepatic cholangiocarcinoma using gadolinium ethoxybenzyl diethylenetriamine pentaacetic acid-enhanced magnetic resonance imaging. J Comput Assist Tomogr 36:704–709. https://doi.org/10.1097/RCT.0b013e3182706562
24. Gabata T, Matsui O, Kadoya M, Yoshikawa J, Ueda K, Kawamori Y, Takashima T, Nonomura A (1998) Delayed MR imaging of the liver: correlation of delayed enhancement of hepatic tumors and pathologic appearance. Abdom Imaging 23:309–313. https://doi.org/10.1007/s002619900347